

Exciton-polaritons in CsPbBr₃ crystals revealed by optical reflectivity in high magnetic fields and two-photon spectroscopy

Dmitri R. Yakovlev,^{1,*} Scott A. Crooker,² Marina A. Semina,³ Janina Rautert,¹ Johannes Mund,¹ Dmitry N. Dirin,^{4,5} Maksym V. Kovalenko,^{4,5} and Manfred Bayer¹

¹*Experimentelle Physik 2, Technische Universität Dortmund, 44227 Dortmund, Germany*

²*National High Magnetic Field Laboratory, Los Alamos National Lab, Los Alamos, New Mexico 87545, USA*

³*Ioffe Institute, Russian Academy of Sciences, 194021 St. Petersburg, Russia*

⁴*Laboratory of Inorganic Chemistry, Department of Chemistry and Applied Biosciences, ETH Zürich, CH-8093 Zürich, Switzerland*

⁵*Laboratory for Thin Films and Photovoltaics, Department of Advanced Materials and Surfaces, Empa - Swiss Federal Laboratories for Materials Science and Technology, CH-8600 Dübendorf, Switzerland*

(Dated: July 17, 2023)

Cesium lead bromide (CsPbBr₃) is a representative material of the emerging class of lead halide perovskite semiconductors that possess remarkable optoelectronic properties. Its optical properties in the vicinity of the band gap energy are greatly contributed by excitons, which form exciton-polaritons due to strong light-matter interactions. We examine exciton-polaritons in solution-grown CsPbBr₃ crystals by means of circularly-polarized reflection spectroscopy measured in high magnetic fields up to 60 T. The excited 2P exciton state is measured by two-photon absorption. Comprehensive modeling and analysis provides detailed quantitative information about the exciton-polariton parameters: exciton binding energy of 32.5 meV, oscillator strength characterized by longitudinal-transverse splitting of 5.3 meV, damping of 6.7 meV, reduced exciton mass of $0.18m_0$, exciton diamagnetic shift of $1.6 \mu\text{eV}/\text{T}^2$, and exciton Landé factor $g_X = +2.35$. We show that the exciton states can be well described within a hydrogen-like model with an effective dielectric constant of 8.7. From the measured exciton longitudinal-transverse splitting we evaluate the Kane energy of $E_p = 15 \text{ eV}$, which is in reasonable agreement with values of 11.8 – 12.5 eV derived from the carrier effective masses.

Keywords: CsPbBr₃, perovskite semiconductor, exciton-polariton, exciton binding energy, Landé factor, high magnetic fields, two-photon spectroscopy.

Cesium lead bromide (CsPbBr₃) is a fully-inorganic member of the large family of lead halide perovskite semiconductors^{1,2}. This material delivers an outstanding combination of optoelectronic properties, such as long charge carrier diffusion lengths up to $1.3 \mu\text{m}$,³ high carrier mobilities ($10 - 181 \text{ cm}^2 \text{ V}^{-1}\text{s}^{-1}$),^{3,4} low densities of carrier trap states ($3.9 \times 10^{10} \text{ cm}^{-3}$) despite a large density of point defects³, and small carrier effective masses ($0.17m_0 - 0.26m_0$) combined with large polarons⁵. CsPbBr₃ has been recently applied to the fabrication of perovskite solar cells^{6,7}, sensitive visible light detectors⁸, and high-energy detectors^{9,10}. Fully inorganic CsPbBr₃ exhibits higher stability against elevated temperatures and polar solvents compared to analogous lead halide perovskites that incorporate organic cations, e.g., methyl-ammonium (MA) lead bromide. In applications for hard radiation detection, CsPbBr₃ is indispensable as it is the only lead halide perovskite that can operate under the high bias required for efficient extraction of charge carriers¹⁰.

Optical properties of semiconductors in the vicinity of the band gap energy are controlled by excitons, making knowledge of the exciton parameters of great importance for optoelectronics. CsPbBr₃ is a model material for the class of lead halide perovskite semiconductors. It is widely studied experimentally and theoretically,

with initial papers on exciton properties dating back to 1978¹¹⁻¹⁴. Light-matter interactions are quite strong in CsPbBr₃¹⁵⁻¹⁸, which results in a pronounced resonance in reflectivity and absorption spectra in the vicinity of the band gap, with features of exciton-polaritons¹⁹. This interaction can be further enhanced in a microcavity²⁰.

Magneto-optical methods are powerful tools to measure exciton parameters in semiconductors²¹⁻²⁴. Exciton binding energies can be evaluated from the diamagnetic shift of the 1S exciton state in magnetic fields and/or from the observation of excited exciton states (2S, 3S, etc.), which gain oscillator strength and become increasingly visible in high fields. In both cases the exciton linewidth is a critical parameter for the evaluation accuracy, which in turn is improved in high magnetic fields. Magneto-optical studies in high magnetic fields of 45 – 150 T were successfully used for investigation of lead halide perovskite semiconductors²⁵⁻³⁵. Most studies to date were made on polycrystalline films with rather broad exciton lines, and results on single crystals with small inhomogeneous broadening of the excitons are available only for MAPbBr₃³⁵ and MAPbI₃³².

For CsPbBr₃ films, measurements in magnetic fields up to 150 T indicate an exciton binding (Rydberg) energy of 33 meV and a reduced exciton mass of $\mu = 0.126m_0$ ³¹. Note that earlier and not very detailed reports inferred exciton binding energies of 37 meV¹³ and 34 meV³⁶. Importantly, however, CsPbBr₃ has a rich spectrum of optical phonons with energies ranging from 4 to 25 meV^{37,38}, values which are close to, but smaller than, the exciton

binding energy. It is generally in the energy range of the optical phonons where the magnitude of the energy-dependent dielectric constant $\varepsilon(\omega)$ varies significantly between its stationary (i.e. zero-frequency) value (ε_s) and its value in the high-frequency limit (ε_∞). This fact provides two aspects for the exciton properties and calculation of its parameters. The first one is that phenomenologically the exciton energies are often described in the framework of a hydrogen-like model, but with an effective dielectric constant ε_{eff} , which falls between the high frequency and static dielectric constants $\varepsilon_\infty < \varepsilon_{eff} < \varepsilon_s$. The second one is that the dielectric screening of the exciton may, in fact, differ between the exciton ground and excited states due to their different radii³⁹ and, consequently, binding energies, such that the energy spectrum of excited exciton states may not conform to the classic Rydberg series that is predicted by hydrogen-like models (which assume a constant ε_{eff}). Note, that the exciton spectra also can differ from the Rydberg series in semiconductors with complex band structure^{40–42}. Although, in the lead halide perovskites the top valence and bottom conduction bands have a simple structure^{43,44} (see also Figure S1a), making the hydrogenic model a good approximation at first glance.

In this study we check the applicability of the Rydberg formula for excitons in CsPbBr₃ and determine fundamental exciton parameters such as the Rydberg energy, reduced mass, and effective dielectric constant. The reflectivity of light in the optical range of the exciton ground state in high magnetic fields up to 60 T is measured for two circular polarizations of incident light. We model the measured spectra within the exciton-polariton model allowing us to determine with a high accuracy the positions of transverse and longitudinal excitons and their energy splitting, g -factors, and diamagnetic shift. To make the evaluation of exciton parameters more accurate the excited 2P exciton state has also been measured by two-photon excitation in magnetic fields up to 10 T.

RESULTS

The sample under study is a fully inorganic lead halide perovskite bulk crystal of CsPbBr₃ grown in solution (Methods). Information on its optical and spin properties in low magnetic fields can be found in Refs.^{44–46}. Here we focus on exciton-polariton parameters and their modification in strong magnetic fields. Experiments were performed at $T = 1.6$ K, with the sample immersed in pumped liquid helium.

It has been appreciated for decades^{19,24,47,48} that a proper description of excitons interacting with light in semiconductors requires consideration of the exciton-polariton effect, which accounts for the interaction of the mechanical exciton with the light wave. This effect characterizes the dependence of the dielectric function on the wave vector (spatial dispersion) and gives rise to two exciton-polariton modes, which modifies the

optical properties of the semiconductor in the spectral range of the exciton-polariton resonance. The splitting between transverse and longitudinal (with respect to the wave vector) excitons is the consequence of the long-range part of the exchange interaction⁴⁸ and, simultaneously, is connected with the exciton polarizability, describing its oscillator strength and playing the key role in exciton-polariton dispersion relation. Here we analyze the optical reflectivity of CsPbBr₃ crystals in the context of the exciton-polariton model and derive fundamental optoelectronic parameters.

Reflectivity of exciton-polaritons in pulsed magnetic fields.

The reflectivity spectrum of the CsPbBr₃ crystal at zero magnetic field is shown in Figure 1a. It has a pronounced exciton-polariton resonance, which results from the interaction of the mechanical excitons with the photons and their conversion to each other in the crystal. For its model description and fit of the reflectivity spectrum we use the commonly accepted theory of exciton-polaritons^{19,47}, see Supporting Information S2. For the boundary conditions we take the “dead layer” approach introduced by Hopfield and Thomas⁴⁷. Schematically the exciton-polariton dispersion is shown in Fig. 1c. Here, E_T is the energy of the transverse (“mechanical”) exciton, E_L is the energy of the longitudinal exciton, and $\hbar\omega_{LT} = E_L - E_T$ is the longitudinal-transverse splitting, which characterizes the exciton oscillator strength⁴⁹. In Fig. 1c “LP” and “UP” denote lower and upper exciton-polariton branches, dashed line “LE” corresponds to longitudinal exciton, dashed line “TE” to transverse exciton without account of the polariton effect, dotted line shows the light dispersion. In cubic crystals longitudinal excitons are optically inactive and at zero wave vector their energy coincides with the upper polariton branch^{48,50}. Although, CsPbBr₃ in low temperatures is in the orthorhombic phase, which has a lower symmetry than cubic, and, in principle, longitudinal exciton may be observable in optics, in experiment we do not see any line that can be attributed to LE.

The dashed line in Fig. 1a shows the fit of the experimental reflectivity spectrum with Eq. (S4). Here we took the background dielectric constant $\varepsilon_b = 4.3$ ⁵¹ as a high frequency one and the translation exciton mass $M = 0.72m_0$. Note, that the fit does not depend strongly on the value of M , for details see Supporting Information S2. The best fit provides the following exciton-polariton parameters: $E_T = 2.322$ eV, $\hbar\omega_{LT} = 5.3$ meV, exciton damping $\hbar\Gamma = 6.7$ meV, and “dead” layer thickness $L = 2.3$ nm. We note the considerable value of $\hbar\omega_{LT}$, which justifies the account of the polariton effect in modeling the reflectivity spectra of CsPbBr₃.

Reflectivity spectra were measured in pulsed magnetic fields up to 60 T in σ^+ and σ^- circular polarizations in order to distinguish exciton states with spin ± 1 and evaluate the exciton Zeeman splitting and its Landé g -factor (see scheme in Fig. 1d). The spectra measured in $B = 60$ T are shown in Fig. 1b. One can see the

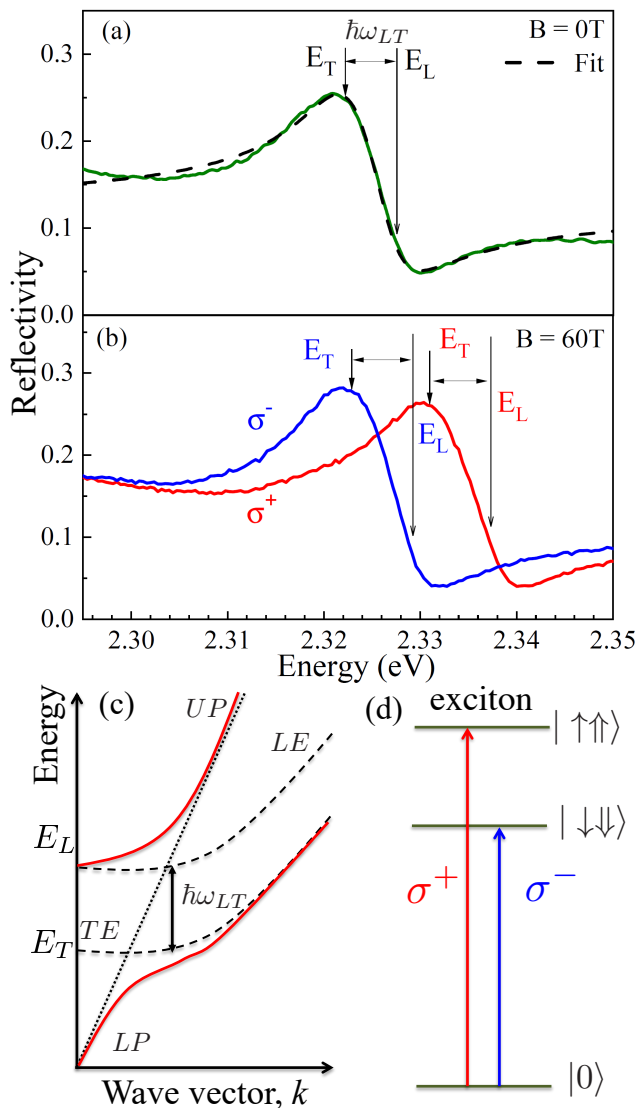


FIG. 1. Reflectivity spectra of CsPbBr₃ in (a) zero and (b) 60 T magnetic field, measured at $T = 1.6$ K. Solid lines are experiment and the dashed line is a fit using $E_T = 2.322$ eV, $\hbar\omega_{LT} = 5.3$ meV, $\hbar\Gamma = 6.7$ meV, and $L = 2.3$ nm. (c) Scheme of the exciton-polariton dispersion that accounts for the spatial dispersion. (d) Scheme of the exciton optical transitions in magnetic field. Single and double arrows correspond to electron and hole spins, respectively, which in optically active exciton states have spin +1 for $|\uparrow\uparrow\rangle$ and -1 for $|\downarrow\downarrow\rangle$. $|0\rangle$ is the ground state of the unexcited crystal.

pronounced Zeeman splitting of the oppositely polarized exciton resonances.

There are three effects of magnetic fields on the exciton resonance that we measured and analyzed: the diamagnetic energy shift (which is same for both spin components), the Zeeman splitting, and the increase of the exciton oscillator strength. In the regime of weak magnetic fields, where the exciton binding energy exceeds the cyclotron energies of the electrons and holes, the energy

of the n -th exciton state in the hydrogen-like model is

$$E_X^{(n)} = E_g - \frac{R^*}{n^2} \pm \frac{1}{2}g_X\mu_B B + c_d^{(n)}B^2. \quad (1)$$

Here E_g is the free-particle band gap energy, g_X the exciton Landé g -factor, and μ_B is the Bohr magneton. Here the plus sign in the Zeeman term $\pm \frac{1}{2}g_X\mu_B B$ corresponds to excitons optically active in σ^+ polarization, and the minus sign corresponds to excitons active in σ^- . R^* is the exciton Rydberg, which is equal to the binding energy of a 1S hydrogen-like exciton ground state E_b^{1S} :

$$R^* = E_b^{1S} = \frac{\mu e^4}{2\hbar^2 \epsilon_{\text{eff}}^2} = \frac{e^2}{2\epsilon_{\text{eff}} a_B}, \quad (2)$$

where μ is the reduced exciton mass, which is composed of the electron and hole effective masses as $\mu^{-1} = m_e^{-1} + m_h^{-1}$, e is the electron charge, \hbar is the Planck constant, ϵ_{eff} is the effective dielectric constant, and a_B is the exciton Bohr radius:

$$a_B = \frac{\hbar^2 \epsilon_{\text{eff}}}{\mu e^2}. \quad (3)$$

The diamagnetic coefficient $c_d^{(n)}$ is given by

$$c_d^{(n)} = \frac{e^2}{8\mu c^2} \langle \rho_n^2 \rangle, \quad (4)$$

where c is speed of light and $\langle \rho_n^2 \rangle$ is the mean square of exciton wave function size in the plane perpendicular to the magnetic field. In the hydrogen-like model for the 1S-state, $\langle \rho_{1S}^2 \rangle = 2a_B^2$ and for the 2P₁₀-state $\langle \rho_{2P}^2 \rangle = 12a_B^2$. The binding energy of the 2P state is 4 times smaller than the binding energy of the 1S state:

$$E_b^{2P} = \frac{\mu e^4}{8\hbar^2 \epsilon_{\text{eff}}^2} = \frac{e^2}{8\epsilon_{\text{eff}} a_B}. \quad (5)$$

We fit the reflectivity spectra measured at all magnetic fields and plot the field dependence of these parameters in Fig. 2. Figure 2a shows the E_T and E_L energies of the exciton states active in σ^+ and σ^- circular polarizations. The energy of E_L we calculate as $E_L = E_T + \hbar\omega_{LT}$. The Zeeman splitting of the exciton states calculated as $E_{\sigma^+} - E_{\sigma^-} = g_X\mu_B B$ is shown in Fig. 2b. The dependences coincide for the E_T and E_L excitons, and their linear fit gives the exciton g -factor $g_X = +2.35$. We emphasize that it is a direct measurement of g_X value and sign, which is positive. This result is in agreement with our recent reports on the universal dependence of exciton⁴⁶ and isolated charge carrier⁴⁴ g -factors on the band gap energy in lead halide perovskite bulk crystals. Note that the high linearity of the field dependence of the Zeeman splitting indicates that band mixing is negligibly small in lead halide perovskites even in very strong magnetic fields. This is explained by the simple spin structure (spin 1/2) of the electron and hole bands in the vicinity of the band gap (which contribute primarily to the exciton wave

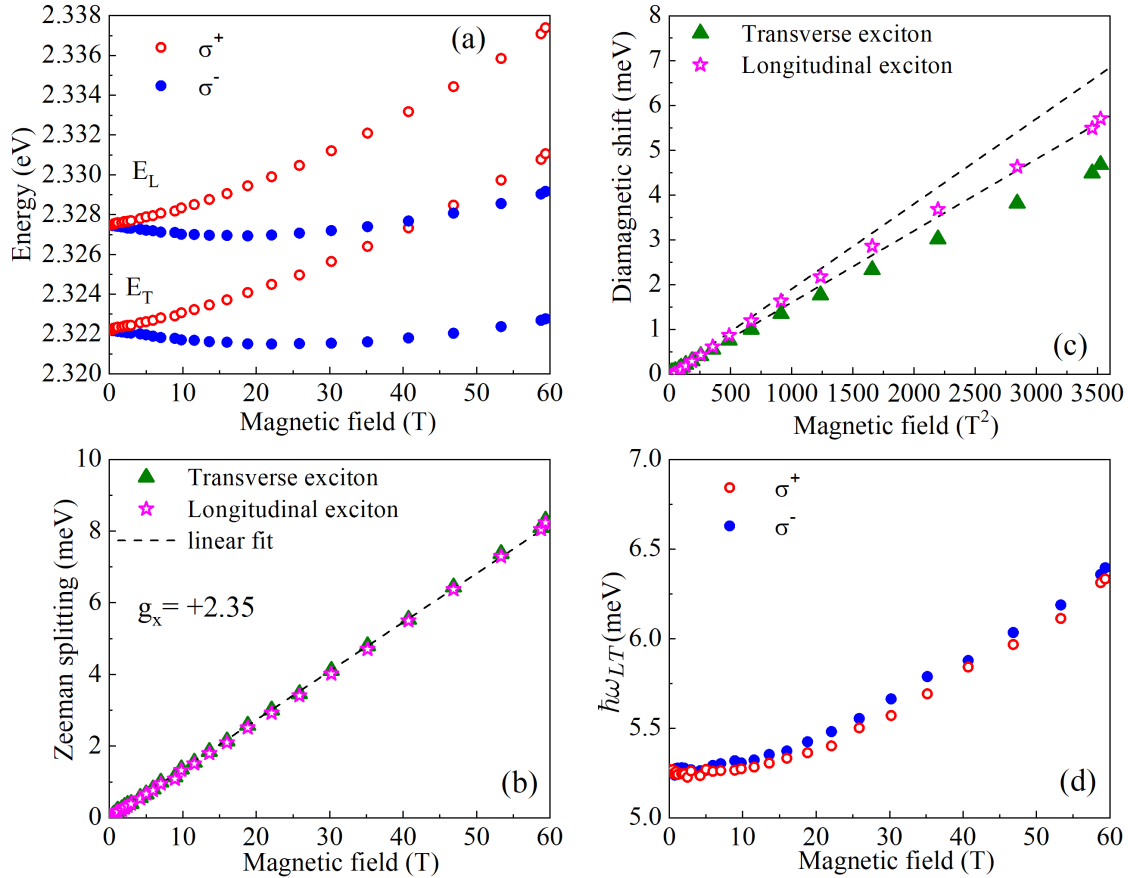


FIG. 2. Parameters of the 1S exciton-polariton in CsPbBr₃ in strong magnetic fields evaluated from polarized reflectivity spectra. $T = 1.6$ K. (a) Energies of transverse (E_T) and longitudinal (E_L) excitons active in σ^+ and σ^- circular polarization as a function of magnetic field. (b) Magnetic field dependence of the Zeeman splitting $E_{\sigma^+} - E_{\sigma^-}$ of transverse (triangles) and longitudinal (open stars) excitons. The dashed line is a linear fit with $g_X = +2.35$. (c) Diamagnetic shift of transverse and longitudinal excitons vs. B^2 . Dashed lines are B^2 fits with $c_d^{1S} = 1.6 \mu\text{eV}/\text{T}^2$ and $c_d^L = 2 \mu\text{eV}/\text{T}^2$, respectively. (d) The longitudinal-transverse splitting in two circular polarizations as a function of magnetic field.

function), and the rather large energy separation to the higher-lying conduction bands.

The diamagnetic shift of the transverse and longitudinal excitons, which was calculated as the center-of-gravity of the σ^\pm components, is shown in Fig. 2c as a function of the square of magnetic field. Dashed lines are B^2 fits; they describe well the experimental data in fields up to 25 T (more details will be given below in Fig. 4). From the fits we evaluate the diamagnetic coefficients for the transverse exciton $c_d^{1S} = 1.6 \mu\text{eV}/\text{T}^2$ and longitudinal exciton $c_d^L = 2 \mu\text{eV}/\text{T}^2$. Their difference originates from the increase of the exciton oscillator strength ($\hbar\omega_{LT}$) with magnetic field, which is shown in Fig. 2d. It increases from 5.3 meV at zero field up to 6.4 meV at $B = 60$ T. The exciton damping $\hbar\Gamma$ does not significantly depend on the magnetic field (not shown here).

Two-photon spectroscopy of 2P exciton state.

Information about excited exciton states enriches the knowledge of the exciton parameters and allows one to define them with higher precision. Unfortunately, the 2S exciton state was not detectable in reflectivity spectra even in strong magnetic fields, most probably due to its small oscillator strength. Therefore, we used another approach and measured the 2P exciton state which is forbidden for one-photon excitation, but is allowed for two-photon excitation. We measured the photoluminescence excitation (PLE) spectrum using two-photon excitation, i.e. the laser photon energy was tuned in the range close to $E_g/2$. Recently, we used this technique to study excitons in CdSe colloidal nanoplatelets⁵².

Figure 3 shows the two-photon PLE spectra of CsPbBr₃ measured in zero magnetic field and in 10 T. One can see a pronounced resonance of the 2P exciton with a maximum at $E_{2P} = 2.3467$ eV at zero magnetic field. At $B = 10$ T the maximum is shifted to 2.3476 eV.

The diamagnetic shift of the 2P state is shown in the inset of Fig. 3. The red line shows a B^2 fit using the diamagnetic coefficient $c_d^{2P} = 10 \mu\text{eV}/\text{T}^2$. Note, that this state corresponds to the $2P_{10}$ state with $m = 1$ (orbital momentum) and $q = 0$ (its projection on the light wave vector) following Ref. 53, where magneto-exciton states are calculated within a hydrogen-like model.

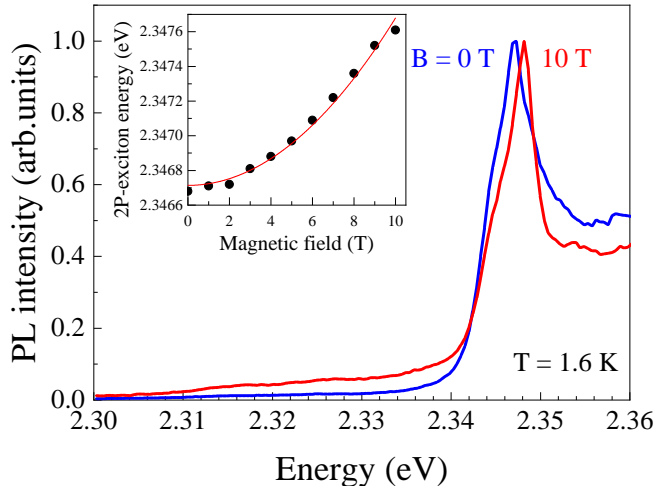


FIG. 3. Two-photon PLE spectra of CsPbBr₃ in zero magnetic field and in 10 T. The PL detection energy is 2.30 eV. Inset: the magnetic field dependence of the 2P-exciton energy. Symbols are experimental data. B^2 fit with diamagnetic coefficient $c_d^{2P} = 10 \mu\text{eV}/\text{T}^2$ is shown by the red line.

Evaluation of exciton parameters.

We now turn to the evaluation of the fundamental exciton parameters which control its ground and excited Rydberg states: binding energy, reduced mass, and effective dielectric constant. There are several challenges involved:

(i) The most straightforward way to measure the exciton Rydberg energy, i.e., the binding energy of its 1S state, would be to measure it as $R^* = E_g - E_T$. But in the studied CsPbBr₃ crystal, similar to other lead halide perovskite crystals and polycrystalline films^{31,34}, the free-particle gap E_g has no pronounced feature in optical spectra. It can, in principle, be evaluated by different means, such as by extrapolation to zero field of the magneto-exciton fan chart measured in strong magnetic fields, but the accuracy of this approach is limited. In Ref. 31 the 1S exciton ground state binding energy was measured by comparing the energy positions of 1S and 2S exciton states. However, the latter was pronounced only in high magnetic fields and its position in zero field was extrapolated.

(ii) As already mentioned, in lead halide perovskites the screening of the Coulomb interaction may be different for different exciton states, and consequently exciton

energies can deviate from the standard hydrogenic Rydberg series.

One approach to estimate the deviation of the binding energies of the exciton states from the hydrogen-like model is based on comparison of the diamagnetic coefficients for the 1S and 2P states. The hydrogen-like model predicts a ratio $c_d^{1S}/c_d^{2P} = 1/6$; see Ref. 53 and Eqs. (8), (9). The experimental values that we obtained here are $c_d^{1S} = 1.6 \mu\text{eV}/\text{T}^2$ and $c_d^{2P} = 10 \mu\text{eV}/\text{T}^2$. Their ratio is 1/6.25, which evidences the good validity of the hydrogen-like model for describing excitons in CsPbBr₃.

For accurate and self-consistent evaluation of the exciton parameters we treat the effective dielectric constant ϵ_{eff} for 1S (ϵ_{1S}) and 2P (ϵ_{2P}) exciton states as independent fitting parameters and determine them separately from the analysis of the experimental data, see SI, S2 for details. We have four parameters to be determined: the exciton reduced mass (μ), the band gap energy (E_g), and the effective dielectric constants for the 1S and 2P states (ϵ_{1S} and ϵ_{2P}). We use, therefore, four experimentally measured values: the diamagnetic coefficients (c_d^{1S} and c_d^{2P}) and exciton resonance energies ($E^{1S} = E_T$, and E^{2P}). We use the four following equations, which link the evaluated and measured parameters.

$$E^{1S} = E_g - E_b^{1S} = E_g - \frac{e^4}{2\hbar^2} \frac{\mu}{\epsilon_{1S}^2}, \quad (6)$$

$$E^{2P} = E_g - E_b^{2P} = E_g - \frac{e^4}{8\hbar^2} \frac{\mu}{\epsilon_{2P}^2}, \quad (7)$$

$$c_d^{1S} = \frac{\hbar^4}{4e^2c^2} \frac{\epsilon_{1S}^2}{\mu^3}, \quad (8)$$

$$c_d^{2P} = \frac{3\hbar^4}{2e^2c^2} \frac{\epsilon_{2P}^2}{\mu^3}. \quad (9)$$

An equal number of evaluated parameters and linear equations provides accurate and unequivocal evaluation of all parameters. The following parameters are determined: $\mu = 0.18m_0$, $E_g = 2.3545 \text{ eV}$, $\epsilon_{1S} = 8.66$, and $\epsilon_{2P} = 8.84$. They bring us to the exciton binding energies of $E_b^{1S} = 32.5 \text{ meV}$ and $E_b^{2P} = 7.8 \text{ meV}$ for the 1S and 2P states, respectively. Note, that the values of ϵ_{1S} and ϵ_{2P} are quite close, therefore it is safe to assume that all the exciton states can be treated within the hydrogen-like model with a single effective dielectric constant $\epsilon_{\text{eff}} \approx 8.7$ with reasonable accuracy. Moreover, the ratio $E_b^{1S}/E_b^{2P} \approx 4.17$ is close to the value of 4 that is predicted by the hydrogen-like model (Eqs. (2) and (5)). From Eq. (3) we get the Bohr radius of the 1S state $a_B^{1S} = 2.55 \text{ nm}$.

In Table I we summarize the parameters measured and evaluated in this work, and further details are given in Supporting Information Table S2.

TABLE I. Exciton parameters in bulk CsPbBr₃ single crystal. $T = 1.6$ K.

Parameter	Value	Comments
$E_T = E^{1S}$	2.3220 eV	Energy of transverse exciton.
E_L	2.3273 eV	Energy of longitudinal exciton.
$\hbar\omega_{LT}$	5.3 meV	Longitudinal-transverse splitting.
$\hbar\Gamma$	6.7 meV	Exciton damping.
$4\pi\alpha_0$	0.0195	Exciton polarizability.
ε_b	4.3	Background dielectric constant. Taken as $\varepsilon_b = \varepsilon_\infty = 4.3$ from Ref. 51.
E^{2P}	2.3467 eV	Energy of the 2P exciton.
g_X	+2.35	Exciton g -factor.
c_d^{1S}	1.6 $\mu\text{eV}/\text{T}^2$	Diamagnetic coefficient of 1S exciton.
c_d^{2P}	10 $\mu\text{eV}/\text{T}^2$	Diamagnetic coefficient of 2P exciton.
E_b^{1S}	32.5 meV	Binding energy of the 1S exciton state, i.e. the exciton Rydberg R^* in hydrogen-like model.
E_b^{2P}	7.8 meV	Binding energy of the 2P exciton state.
E_g	2.3545 eV	Band gap energy.
ε_{eff}	8.7	Effective dielectric constant.
μ	0.18 m_0	Reduced exciton mass.
M	0.72 m_0	Translation exciton mass.
a_B^{1S}	2.55 nm	Bohr radius of the exciton ground state.

DISCUSSION

Let us have a close look at the field-dependent energy shift of the 1S exciton state, plotted in Fig. 2(c) as a function of B^2 and also in Figure 4 as a function of B . In both cases one can see that the pure B^2 shift is valid primarily in magnetic fields weaker than 25 T. Here, the condition for the diamagnetic exciton is fulfilled with high accuracy. Namely, the cyclotron radius of the charge carriers $\sqrt{\hbar c/eB}$ should be larger than the exciton Bohr radius a_B . The critical magnetic field for this criterion is $B_c = \hbar c/(ea_B^2)$. In CsPbBr₃ it gives $B_c \approx 100$ T, which is only a factor of ~ 2 larger than the 60 T fields we use. Therefore we can expect a small deviation from purely quadratic diamagnetic shifts when approaching the high fields used in this work.

The dashed line in Fig. 4 shows the results of a full calculation that accounts for the deviation from the weak magnetic field regime. This simple model Hamiltonian neglects the motion of the exciton center of mass.

$$\hat{H} = \frac{\hbar^2}{2\mu}\Delta - \frac{e^2}{\varepsilon_{\text{eff}}r} + \frac{1}{8} \frac{e^2 B^2}{c^2 \mu} (x^2 + y^2). \quad (10)$$

Here Δ is the Laplace operator, acting on the electron and hole relative coordinate \mathbf{r} , and x and y are components of \mathbf{r} in the plane perpendicular to the magnetic field. Equation (10) was solved numerically. We used values of $\mu = 0.18m_0$ and $\varepsilon_{\text{eff}} \approx 8.7$ that were determined above. One can see an excellent agreement with experiment in the whole range of measured magnetic fields, which justifies our assumptions made for the calculation of exciton parameters and shows the consistency of the obtained set of exciton parameters.

The exciton parameters measured in this study allow us to estimate the Kane energy E_p , which is connected

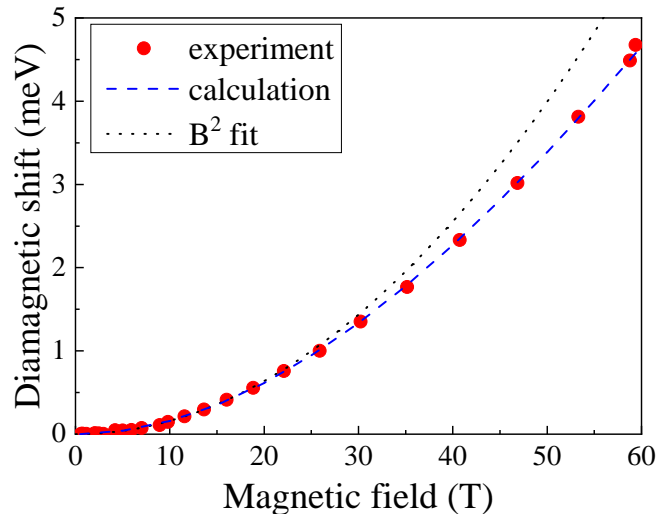


FIG. 4. The 1S-exciton shift in magnetic field measured (circles), calculated with Eq. (10) (dashed line) and B^2 fit (dotted line). $\mu = 0.18m_0$ and $\varepsilon_{\text{eff}} = 8.7$.

with the interband momentum matrix element P_{cv} as $E_p = 2P_{cv}^2/m_0$. The Kane energy characterizes the efficiency of the light interaction with the crystal, for details see Supporting Information S3^{44,54,55}. We have two ways to do that. In the first approach, we estimate E_p from the electron and hole effective masses^{44,55}. In lead halide perovskites the electron and hole effective masses are similar⁵⁶, therefore we estimate $m_h = 2\mu$, which for $\mu = 0.18m_0$ gives $m_h = 0.36m_0$. Then taking the band gap energy of CsPbBr₃ of $E_g = 2.35$ eV and the conduction band spin orbit splitting $\Delta_{SO} = 1.5$ eV⁴⁴ we get from Eq. (S13) $E_p = 11.8 - 12.5$ eV. The two values results from evaluations via the electron and hole effective

masses.

We made a second evaluation of E_p from the link between the longitudinal-transverse splitting and E_p given by²³:

$$\hbar\omega_{LT} = \frac{4e^2\hbar^2}{3m_0E_T^2} \frac{E_p}{\varepsilon_b a_B^3}. \quad (11)$$

Using parameters from Table I, we calculate $E_p = 15$ eV, which is close to the value from the first evaluation. This agreement justifies use of the exciton-polariton approach and obtained exciton parameters. Note that due to the difference of the band structure of the lead halide perovskites and conventional zinc-blende semiconductors, for the latter in Eq. (11) the coefficient 2 should be used instead of 4/3.

The following evaluations of E_p can be made on the basis of literature data. In Ref. [44] the effective masses of electrons and holes were calculated by DFT and ETB methods, the reported values are $m_e = 0.3(0.291)m_0$ and $m_h = 0.26(0.298)$ for DFT (ETB), respectively. Also the experimental value for hole effective mass $m_h = 0.26m_0$ was measured by angle-resolved photoelectron spectroscopy in Ref. [5]. They correspond to a reduced exciton mass $\mu = 0.14 - 0.15$ and a Kane energy $E_p = 13.5 - 17.5$ eV. In Ref. [44] from the modeling of the universal dependence of the charge carrier g -factors on the band gap energy, the parameter $P_{cv} = \hbar p/m_0 = 6.8$ eVÅ was evaluated. It corresponds to a Kane energy $E_p = 12.1$ eV.

Magneto-optical experiments in high fields up to 70 T were reported for CsPbBr₃ polycrystalline films in Ref. 31. The following exciton parameters were evaluated: $R^* = E_b^{1S} = 33 \pm 1$ meV, $\mu = (0.126 \pm 0.01)m_0$, and $\varepsilon_{eff} = 7.8$. The exciton binding energy of the 1S state, estimated as the difference between the energy of the 1S exciton and extrapolation of the magneto-exciton fan chart to get E_g , is very close to our value of 32.5 meV. While the reduced exciton mass, evaluated from the fit of the fan chart in strong magnetic fields, is smaller than our determination of $\mu = 0.18m_0$, which is based on diamagnetic shifts in fields below 25 T, it can be measured with high accuracy due to the narrow exciton lines in bulk crystals. The ε_{eff} evaluated in Ref. 31 from E_b^{1S} and μ is smaller than our value of 8.7, which is related to the smaller μ value. The band gap energy of $E_g = 2.3545$ eV that we determine in our study is in line with the literature data^{6,31,57}.

CONCLUSIONS

Magneto-optics and two-photon spectroscopy of CsPbBr₃ crystals allow us to determine a detailed set of exciton and exciton-polariton parameters summarized in Table I. The combination of these approaches can be readily extended to other lead halide perovskites and their nanostructures.

METHODS

Samples. The CsPbBr₃ crystals were grown with a slight modification of the inverse temperature crystallization technique, see Ref.⁵⁸. First, CsBr and PbBr₂ were dissolved in dimethyl sulfoxide. Afterwards a cyclohexanol in N,N-dimethylformamide solution was added. The resulting mixture was heated in an oil bath to 105°C whereby slow crystal growth occurs. The obtained crystals were taken out of the solution and quickly loaded into a vessel with hot (100°C) N,N-dimethylformamide. Once loaded, the vessel was slowly cooled down to about 50°C. After that, the crystals were isolated, wiped with filter paper and dried. The obtained rectangular-shaped CsPbBr₃ is crystallized in the orthorhombic modification. The crystals have one selected (long) side along the c -axis [001] and two nearly identical sides along the $[\bar{1}10]$ and [110] axes⁵⁹.

Reflectivity in pulsed magnetic fields. The sample was mounted on a custom fiber-coupled probe in a helium bath cryostat with a long tail extending into the bore of a 65 T pulsed magnet. The experiments were performed at a temperature of $T = 1.6$ K, with the sample immersed in superfluid helium. Broadband white light from a halogen lamp was coupled down a 100 μ m diameter multimode optical fiber, and light reflected from the sample was collected by a 600- μ m diameter fiber. The light wavevector \mathbf{k} was perpendicular to the sample surface and parallel to B (Faraday geometry). Thin film circular polarizers were used to select σ^- and σ^+ polarized light. Full optical spectra were acquired every 1 ms continuously throughout the magnet pulse using a fast charge-coupled-device (CCD) camera combined with a 0.3-meter spectrometer. To switch between σ^- and σ^+ polarization, the direction of the magnetic field was switched. Further details of these methods can be found in Ref. 60.

Two-photon excitation of photoluminescence. In order to obtain information on the energy of the 2P exciton state in absorption, we measured photoluminescence excitation (PLE) spectra. In this technique the emission was detected at the low energy tail of the PL spectrum and the laser photon energy was tuned across the exciton absorption spectral range. For excitation a pulsed laser system with an optical parametric amplifier (OPA) was used. Its photon energy was tunable in the spectral range of 0.5 – 4.0 eV. The laser pulses had a duration of 2.5 ps, a linewidth of 0.23 nm, and a repetition frequency of 30 kHz. For the two-photon PLE the laser was tuned in the range of 1.15–1.20 eV. The PL was measured at 2.30 eV, about 50 meV below the exciton energy. For this, it was spectrally selected by a 10 nm wide band-pass filter and a spectrometer. For these measurements the sample was placed in the magneto-optical cryostat with direct optical access. The sample was in direct contact with pumped liquid helium at $T = 1.6$ K. Static magnetic fields up to 10 T were generated by a split-coil superconducting magnet and applied in the Faraday

geometry.

ASSOCIATED CONTENT

Supporting Information. Additional information on the band structure and exciton fine structure in CsPbBr₃. Theoretical consideration of the exciton-polaritons in reflectivity spectra. Table with detailed comments on evaluation of exciton parameters.

AUTHOR INFORMATION

Corresponding Author

Dmitri R. Yakovlev, Email: dmitri.yakovlev@tu-dortmund.de

ORCID

Dmitri R. Yakovlev: 0000-0001-7349-2745
 Scott A. Crooker: 0000-0001-7553-4718
 Marina A. Semina: 0000-0003-3796-2329
 Janina Rautert: 0000-0002-9908-4851
 Johannes Mund: 0000-0002-8022-7584
 Dmitry N. Dirin: 0000-0002-5187-4555
 Maksym V. Kovalenko: 0000-0002-6396-8938
 Manfred Bayer: 0000-0002-0893-5949

Notes

The authors declare no competing financial interests.

Acknowledgments

The authors are thankful to M. M. Glazov and E. L. Ivchenko for fruitful discussions and to P. Sercel for valuable advice. The authors acknowledge financial support

of the Deutsche Forschungsgemeinschaft through the Collaborative Research Center TRR142 (Project A11) and the Priority Programme SPP2196 (Project YA 65/26-1). M.A.S. acknowledges support of the Russian Science Foundation (project 23-12-00300). The National High Magnetic Field Laboratory is supported by the National Science Foundation DMR-1644779, the State of Florida, and the US Department of Energy. S.A.C. acknowledges support from the US Department of Energy “Science of 100 T” program. Work at ETH Zürich (D.N.D. and M.V.K.) was financially supported by the Swiss National Science Foundation (grant agreement 186406, funded in conjunction with SPP219 through DFG-SNSF bilateral program) and by ETH Zürich through ETH+ Project SynMatLab.

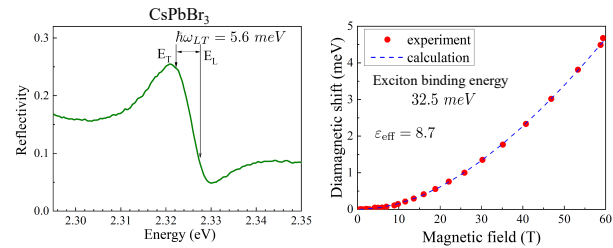


FIG. 5. TOC figure.

* dmitri.yakovlev@tu-dortmund.de

¹ *Hybrid Organic Inorganic Perovskites: Physical Properties and Applications*, eds. Vardeny, Z. V.; Beard, M. C. World Scientific, **2022**.

² *Halide Perovskites for Photonics*, eds. Vinattieri, A.; Giorgi, G. AIP Publishing, Melville, New York, **2021**.

³ Fan, Z.; Liu, J.; Zuo, W.; Liu, G.; He, X.; Luo, K.; Ye, Q.; Liao, C. Solution-processed MAPbBr₃ and CsPbBr₃ single-crystal detectors with improved X-ray sensitivity via interfacial engineering. *Phys. Stat. Sol. (a)* **2020**, *217*, 2000104.

⁴ Zhang, Z.; Saporov, B. Charge carrier mobility of halide perovskite single crystals for ionizing radiation detection. *Appl. Phys. Lett.* **2021**, *119*, 030502.

⁵ Puppini, M.; Polishchuk, S.; Colonna, N.; Crepaldi, A.; Dirin, D. N.; Nazarenko, O.; De Gennaro, R.; Gatti, G.; Roth, S.; Barillot, T.; Poletto, L.; Xian, R. P.; Rettig, L.; Wolf, M.; Ernstorfer, R.; Kovalenko, M. V.; Marzari, N.; Griioni, M.; Chergui, M. Evidence of large polarons in photoemission band mapping of the perovskite semiconductor CsPbBr₃. *Phys. Rev. Lett.* **2020**, *124*, 206402.

⁶ Kulbak, M.; Cahen, D.; Hodes, G. How important is the organic part of lead halide perovskite photovoltaic cells? Efficient CsPbBr₃ cells. *J. Phys. Chem. Lett.* **2015**, *6*, 2452.

⁷ Kulbak, M.; Gupta, S.; Kedem, N.; Levine, I.; Bendikov, T.; Hodes, G.; Cahen, D. Cesium enhances long-term stability of lead bromide perovskite-based solar cells. *J. Phys. Chem. Lett.* **2016**, *7*, 167.

- ⁸ Song, J.; Xu, L.; Li, J.; Xue, J.; Dong, Y.; Li, X.; Zeng, H. Monolayer and few-layer all-inorganic perovskites as a new family of two-dimensional semiconductors for printable optoelectronic devices. *Adv. Mater.* **2016**, *28*, 4861.
- ⁹ Matt, G. J.; Levchuk, I.; Knüttel, J.; Dallmann, J.; Osvet, A.; Sytnyk, M.; Tang, X.; Elia, J.; Hock, R.; Heiss, W.; Brabec, C. J. Sensitive direct converting X-ray detectors utilizing crystalline CsPbBr₃ perovskite films fabricated via scalable melt processing. *Adv. Mater. Interfaces* **2020**, *7*, 1901575.
- ¹⁰ Stoumpos, C.; Malliakas, C. D.; Peters, J. A.; Liu, Z.; Sebastian, M.; Im, J.; Chasapis, Th. C.; Wibowo, A. C.; Chung, D. Y.; Freeman, A. J.; Wessels, B. W.; Kanatzidis, M. G. Crystal growth of the perovskite semiconductor CsPbBr₃: A new material for high energy radiation detection. *Crystal Growth & Design* **2013**, *13*, 2722.
- ¹¹ Heidrich, K.; Künzel, H.; Treusch, J. Optical properties and electronic structure of CsPbCl₃ and CsPbBr₃. *Solid State Commun.* **1978**, *25*, 887–889.
- ¹² Ito, H.; Onuki, H.; Onaka, R. Optical and photoelectronic studies of CsPbCl₃ and CsPbBr₃. *J. Phys. Soc. Japan* **1978**, *45*, 2043–2044.
- ¹³ Fröhlich, D.; Heidrich, K.; Künzel, H.; Trendel, G.; Treusch, J. Cesium-trihalogen-plumbates a new class of ionic semiconductors. *J. Luminescence* **1979**, *18/19*, 385–388.
- ¹⁴ Heidrich, K.; Schäfer, W.; Schreiber, M.; Söchtig, J.; Trendel, G.; Treusch, J.; Grandke, T.; Stolz, H. J. Electronic structure, photoemission spectra, and vacuum-ultraviolet

- optical spectra of CsPbCl₃ and CsPbBr₃. *Phys. Rev. B* **1981**, *24*, 5642.
- 15 Su, R.; Ghosh, S.; Wang, J.; Liu, S.; Diederichs, C.; Liew, T. C. H.; Xiong, Q. Observation of exciton polariton condensation in a perovskite lattice at room temperature. *Nature Physics* **2020**, *16*, 301.
 - 16 Su, R.; Fieramosca, A.; Zhang, Q.; Nguyen, H. S.; Deleporte, E.; Chen, Z.; Sanvitto, D.; Liew, T. C. H.; Xiong, Q. Perovskite semiconductors for room-temperature exciton-polaritonics. *Nature Materials* **2021**, *20*, 1315.
 - 17 Tao, R.; Peng, K.; Haeberlé, L.; Li, Q.; Jin, D.; Fleming, G. R.; Kéna-Cohen, S.; Zhang, X.; Bao, W. Halide perovskites enable polaritonic XY spin Hamiltonian at room temperature. *Nature Materials* **2022**, *21*, 761.
 - 18 Dursun, I.; Zheng, Y.; Guo, T.; De Bastiani, M.; Turedi, B.; Sinatra, L.; Haque, M. A.; Sun, B.; Zhumekenov, A. A.; Saidaminov, M. I.; García de Arquer, F. P.; Sargent, E. H.; Wu, T.; Gartstein, Y. N.; Bakr, O. M.; Mohammed, O. F.; Malko, A. V. Efficient photon recycling and radiation trapping in cesium lead halide perovskite waveguides. *ACS Energy Lett.* **2018**, *3*, 1492.
 - 19 Klingshirm, C. *Semiconductor Optics* (Springer-Verlag, Berlin 2005).
 - 20 Bao, W.; Liu, X.; Xue, F.; Zheng, F.; Tao, R.; Wang, S.; Xia, Y.; Zhao, M.; Kim, J.; Yang, S.; Li, Q.; Wang, Y.; Wang, Y.; Wang, L.-W.; MacDonald, A. H.; Zhang, X. Observation of Rydberg exciton polaritons and their condensate in a perovskite cavity. *PNAS* **2019**, *116*, 20274–20279.
 - 21 Seisyan, R. P.; Zakharchenya, B. P. Interband magneto-optics of semiconductors as diamagnetic exciton spectroscopy, Chapter 7 in *Landau Level Spectroscopy*, eds. Landwehr, G.; Rashba, E. I. (Elsevier Science Publishers B.V., 1991), pp. 347–443.
 - 22 Seisyan, R. P. Diamagnetic excitons and exciton magnetopolaritons in semiconductors. *Semicond. Sci. Technol.* **2012**, *27*, 053001.
 - 23 Ivchenko, E. L. *Optical Spectroscopy of Semiconductor Nanostructures* (Springer, Berlin 2007).
 - 24 Reynolds, D. C.; Collings, T. C. *Excitons. Their Properties and Uses*. (Academic Press, New York 1981).
 - 25 Kataoka, T.; Kondo, T.; Ito, R.; Sasaki, S.; Uchida, K.; Miura, N. Magneto-optical study on excitonic spectra in (C₆H₁₃NH₃)₂PbI₄. *Phys. Rev. B* **1993**, *47*, 2010–2018.
 - 26 Hirasawa, M.; Ishihara, T.; Goto, T.; Uchida, K.; Miura, N. Magnetoabsorption of the lowest exciton in perovskite-type compound (CH₃NH₃)PbI₃. *Physica B* **1994**, *201*, 427–430.
 - 27 Tanaka, K.; Takahashi, T.; Ban, T.; Kondo, T.; Uchida, K.; Miura, N. Comparative study on the excitons in lead-halide-based perovskite-type crystals CH₃NH₃PbBr₃, CH₃NH₃PbI₃. *Solid State Commun.* **2003**, *127*, 619–623.
 - 28 Tanaka, K.; Takahashi, T.; Kondo, T.; Umeda, K.; Ema, K.; Umebayashi, T.; Asai, K.; Uchida, K.; Miura, N. Electronic and excitonic structures of inorganic-organic perovskite-type quantum-well crystal (C₄H₉NH₃)₂PbBr₄. *Jap. J. Appl. Phys.* **2005**, *44*, 5923–5932.
 - 29 Miyata, A.; Mitioglu, A.; Plochocka, P.; Portugall, O.; Tse-Wei Wang, J.; Stranks, S. D.; Snaith, H. J.; Nicholas, R. J. Direct measurement of the exciton binding energy and effective masses for charge carriers in an organic-inorganic tri-halide perovskite. *Nature Physics* **2015**, *11*, 582–588.
 - 30 Galkowski, K.; Mitioglu, A.; Miyata, A.; Plochocka, P.; Portugall, O.; Eperon, G. E.; Wang, J. T.-W.; Stergiopoulou, T.; Stranks, S. D.; Snaith, H. J.; Nicholas, R. J. Determination of the exciton binding energy and effective masses for methylammonium and formamidinium lead trihalide perovskite semiconductors. *Energy Environ. Sci.* **2016**, *9*, 962–970.
 - 31 Yang, Z.; Surrente, A.; Galkowski, K.; Miyata, A.; Portugall, O.; Sutton, R. J.; Haghighirad, A. A.; Snaith, H. J.; Maude, D. K.; Plochocka, P.; Nicholas, R. J. Impact of the halide cage on the electronic properties of fully inorganic cesium lead halide perovskites. *ACS Energy Lett.* **2017**, *2*, 1621.
 - 32 Yang, Z.; Surrente, A.; Galkowski, K.; Bruyant, N.; Maude, D. K.; Haghighirad, A. A.; Snaith, H. J.; Plochocka, P.; Nicholas, R. J. Unraveling the exciton binding energy and the dielectric constant in single-crystal methylammonium lead triiodide perovskite. *J. Phys. Chem. Lett.* **2017**, *8*, 1851.
 - 33 Baranowski, M.; Plochocka, P.; Su, R.; Legrand, L.; Barisien, T.; Bernardot, F.; Xiong, Q.; Testelin, C.; Chamarro, M. Exciton binding energy and effective mass of CsPbCl₃: A magneto-optical study. *Photon. Res.* **2020**, *8*, A50–A55.
 - 34 Baranowski, M.; Plochocka, P. Excitons in metal halide perovskites. *Advanced Energy Materials* **2020**, *10*, 1903659.
 - 35 Baranowski, M.; Galkowski, K.; Surrente, A.; Urban, J.; Kłopotowski, L.; Maćkowski, S.; Maude, D. K.; Ben Aich, R.; Boujdaria, K.; Chamarro, M.; Testelin, C.; Nayak, P. K.; Dollmann, M.; Snaith, H. J.; Nicholas, R. J.; Plochocka, P. Giant fine structure splitting of the bright exciton in a bulk MAPbBr₃ single crystal. *Nano Lett.* **2019**, *19*, 7054–7061.
 - 36 Pashuk, I. P.; Pidzyrailo, N. S.; Matsko, M. G. Exciton absorption, luminescence, and resonance Raman scattering of light in CsPbCl₃ and CsPbBr₃ crystals at low temperatures. *Sov. Phys. Solid State* **1981**, *23*, 1263–1265.
 - 37 Zhou, X.; Zhang, Z. Electron-phonon coupling in CsPbBr₃. *AIP Advances* **2020**, *10*, 125015.
 - 38 Guo, Y.; Yaffe, O.; Hull, T. D.; Owen, J. S.; Reichman, D. R.; Brus, L. E. Dynamic emission Stokes shift and liquid-like dielectric solvation of band edge carriers in lead-halide perovskites. *Nature Communications* **2019**, *10*, 1175.
 - 39 Franceschetti, A.; Wang, L. W.; Fu, H.; Zunger, A. Short-range versus long-range electron-hole exchange interactions in semiconductor quantum dots. *Phys. Rev. B* **1998**, *58*, R13367(R).
 - 40 Baldereschi A.; Lipari, N.O. Energy levels of direct excitons in semiconductors with degenerate bands. *Phys. Rev. B* **1971**, *3*, 439.
 - 41 Baldereschi A.; Lipari, N.O. Spherical model of shallow acceptor states in semiconductors. *Phys. Rev. B* **1973**, *8*, 2697.
 - 42 Baldereschi A.; Lipari, N.O. Cubic contributions to the spherical model of shallow acceptor states. *Phys. Rev. B* **1974**, *9*, 1525.
 - 43 Even, J.; Pedesseau, L.; Dupertuis, M.-A.; Jancu, J.-M.; Katan, C. Electronic model for self-assembled hybrid organic/perovskite semiconductors: Reverse band edge electronic states ordering and spin-orbit coupling. *Phys. Rev. B* **2012**, *86*, 205301.
 - 44 Kirstein, E.; Yakovlev, D. R.; Glazov, M. M.; Zhukov, E. A.; Kudlacik, D.; Kalitukha, I. V.; Sapega, V. F.; Dimitriev, G. S.; Semina, M. A.; Nestoklon, M. O.; Ivchenko, E. L.; Kopteva, N. E.; Dirin, D. N.; Nazarenko, O.; Ko-

- valenko, M. V.; Baumann, A.; Höcker, J.; Dyakonov, V.; Bayer, M. The Landé factors of electrons and holes in lead halide perovskites: universal dependence on the band gap. *Nat. Commun.* **2022**, *13*, 3062.
- ⁴⁵ Belykh, V. V.; Yakovlev, D. R.; Glazov, M. M.; Grigoryev, P. S.; Hussain, M.; Rautert, J.; Dirin, D. N.; Kovalenko, M. V.; Bayer, M. Coherent spin dynamics of electrons and holes in CsPbBr₃ perovskite crystals. *Nature Commun.* **2019**, *10*, 673.
- ⁴⁶ Kopteva, N. E.; Yakovlev, D. R.; Kirstein, E.; Zhukov, E. A.; Kudlacik, D.; Kalitukha, I. V.; Sapega, V. F.; Hordiiichuk, O.; Dirin, D. N.; Kovalenko, M. V.; Baumann, A.; Höcker, J.; Dyakonov, V.; Crooker, S. A.; Bayer, M. Weak dispersion of exciton Landé factor with band gap energy in lead halide perovskites: Approximate compensation of the electron and hole dependences. *CondMat arXiv* <https://doi.org/10.48550/arXiv.2301.12775> (31.01.2023).
- ⁴⁷ Hopfield, J. J.; Thomas, D. G. Theoretical and experimental effects of spatial dispersion on the optical properties of crystals. *Phys. Rev.* **1963**, *132*, 563.
- ⁴⁸ Andreani, L. C.; Bassani, F.; Quattropani, A. Longitudinal-transverse splitting in Wannier excitons and polariton states. *il Nuovo Cimento D* **1988**, *10*, 1473.
- ⁴⁹ Denisov, M. M.; Makarov, V. P. Longitudinal and transverse excitons in semiconductors. *Phys. Stat. Sol. (b)* **1973**, *56*, 9.
- ⁵⁰ Hopfield, J. J.; Thomas, D. G. On some observable properties of longitudinal excitons. *J. Phys. Chem. Solids* **1960**, *12*, 276-284.
- ⁵¹ Miyata, K.; Meggiolaro, D.; Trinh, M. T.; Joshi, P. P.; Mosconi, E.; Jones, S. C.; De Angelis, F.; Zhu, X.-Y. Large polarons in lead halide perovskites. *Sci. Adv.* **2017**, *3*, e1701217.
- ⁵² Shornikova, E. V.; Yakovlev, D. R.; Gippius, N. A.; Qiang, G.; Dubertret, B.; Khan, A. H.; Di Giacomo, A.; Moreels, I.; Bayer, M. Exciton binding energy in CdSe nanoplatelets measured by one- and two-photon absorption. *Nano Lett.* **2021**, *21*, 10525-10531.
- ⁵³ Makado, P. C.; McGill, N. C. Energy levels of a neutral Hydrogen-like system in a constant magnetic field of arbitrary strength. *J. Phys. C: Solid State Phys.* **1986**, *19*, 873.
- ⁵⁴ Kane, E. O. Band structure of indium antimonide. *J. Phys. Chem. Sol.* **1957**, *1*, 249.
- ⁵⁵ Yu, Z. G. Effective-mass model and magneto-optical properties in hybrid perovskites. *Scientific Reports* **2016**, *6*, 28576.
- ⁵⁶ Becker, M. A.; Vaxenburg, R.; Nedelcu, G.; Sercel, P. C.; Shabaev, A.; Mehl, M. J.; Michopoulos, J. G.; Lambrakos, S. G.; Bernstein, N.; Lyons, J. L.; Stöferle, T.; Mahrt, R. F.; Kovalenko, M. V.; Norris, D. J.; Rain, G.; Efros, Al. L. Bright triplet excitons in caesium lead halide perovskites. *Nature* **2018**, *553*, 189. In Supporting Information.
- ⁵⁷ Hoffman, J. B.; Schleper, A. L.; Kamat, P. V. Transformation of sintered CsPbBr₃ nanocrystals to cubic CsPbI₃ and gradient CsPbBr_xI_{3-x} through halide exchange. *J. Am. Chem. Soc.* **2016**, *138*, 8603.
- ⁵⁸ Dirin, D. N.; Cherniukh, I.; Yakunin, S.; Shynkarenko, Y.; Kovalenko, M. V. Solution-grown CsPbBr₃ perovskite single crystals for photon detection. *Chemistry of Materials* **2016**, *28*, 8470-8474.
- ⁵⁹ Feng, Y.; Pan, L.; Wei, H.; Liu, Y.; Ni, Zh.; Zhao, J.; Rudd, P. N.; Cao, L. R.; Huang, J. Low defects density CsPbBr₃ single crystals grown by an additive assisted method for gamma-ray detection. *J. Mater. Chem. C* **2020**, *8*, 11360-11368.
- ⁶⁰ Stier, A. V.; McCreary, K. M.; Jonker, B. T.; Kono, J.; Crooker, S. A. Exciton diamagnetic shifts and valley Zeeman effects in monolayer WS₂ and MoS₂ to 65 Tesla. *Nat. Commun.* **2016**, *7*, 10643.

SUPPORTING INFORMATION

Exciton-polaritons in CsPbBr₃ crystals revealed by optical reflectivity in high magnetic fields and two-photon spectroscopy

Dmitri R. Yakovlev, Scott A. Crooker, Marina A. Semina, Janina Rautert, Johannes Mund, Dmitry N. Dirin, Maksym V. Kovalenko, Manfred Bayer

S1. Band structure and excitons in orthorhombic CsPbBr₃

Bulk CsPbBr₃ can exist in three structural crystalline phases: the high symmetry cubic (O_h point symmetry) phase, which is stable at temperatures higher than 133°C; the tetragonal (D_{4h}) phase is stable between 133°C and 88°C; and the orthorhombic (D_{2h}) phase stable below 88°C^{S1}. In the tetragonal and orthorhombic phases the direct band transitions are realized at the Γ point of the Brillouin zone, while in the cubic phase the direct band transition is at the R point of the Brillouin zone (corner of the cube).

The band structure of CsPbBr₃ is “inverted” in comparison to conventional III-V and II-VI semiconductors such as GaAs or ZnSe^{S2,S3}. The conduction band in CsPbBr₃ consists of two subbands having net angular momentum $J_e = 3/2$ and $J_e = 1/2$, while the valence band is characterized solely by spin $J_h = 1/2$. The valence band is two-fold degenerate by spin and originates mostly from the overlap of the Pb metal $6s$ -orbitals and the Br $4p$ -orbitals. Spin-orbit coupling does not affect the valence band, although for the lower symmetry in the tetragonal and orthorhombic phases the reduction of symmetry results in effective crystal fields contributing to the valence band dispersion. The conduction band is formed mostly by the Pb $6p$ -orbitals and it is dominated by strong spin-orbit coupling due to the rather large atomic weight of Pb. This leads to a splitting of the conduction band into $J_e = 3/2$, which is split by crystal field in tetragonal and orthorhombic phases, and $J_e = 1/2$ subbands. The lowest conduction subband is the split-off $J_e = 1/2$ subband. A sketch of the band structure of CsPbBr₃ is shown in Fig. S1a. In this figure E_g is the band gap energy, Δ_{le} and Δ_{he} are the splittings between bottom conduction band and the bands of light and heavy electrons (le and he), respectively.

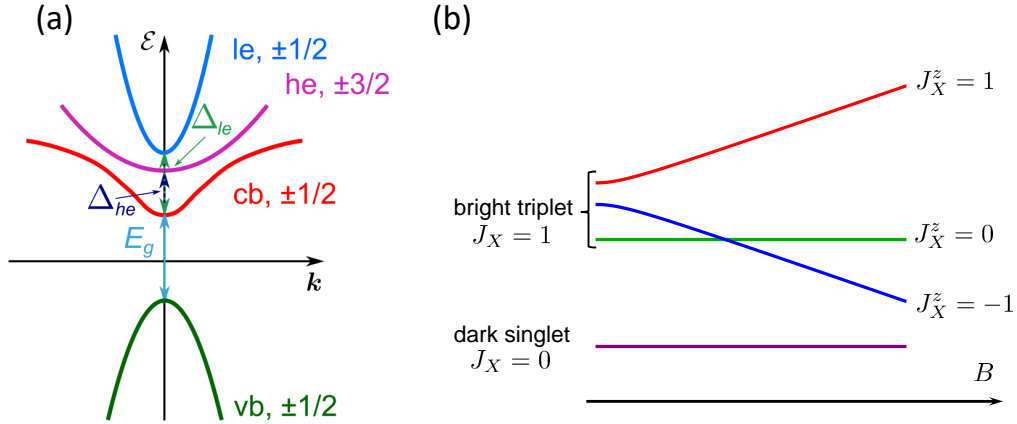


FIG. S1. (a) Schematics of the band structure of CsPbBr₃ in the orthorhombic phase. (b) The scheme of exciton levels in magnetic field.

The band edge excitons in CsPbBr₃ are formed by the Coulomb interaction between a hole with $J_h = 1/2$ at the top of the valence band and an electron with $J_e = 1/2$ at the bottom of the lowest conduction subband. The exciton ground state (which in a hydrogen-like model would have S-like envelope function of electron-hole relative motion), is split by the electron-hole exchange interaction and the Rashba effect into a singlet dark state with net angular momentum $J_X = 0$, and an optically active triplet state with $J_X = 1$. The lowest exciton state is the dark singlet state. The triplet state is fully split in the lower symmetry orthorhombic phase by the spin projection J_X^z on the c -axis direction ([001]). Two of them with $J_X^z = \pm 1$ are active in the Faraday geometry with magnetic field being directed along the [001] direction^{S4}. The exciton fine structure in bulk CsPbBr₃ has not been measured yet. The data for bulk MAPbBr₃ shows values $\sim 200 \mu\text{eV}$ for the bright exciton fine structure splitting^{S4} and we assume similar values for CsPbBr₃. The scheme of exciton levels in applied magnetic field is shown in Fig. S1b. The order of exciton states within the bright triplet and the relative energy splittings are arbitrary. The magnitudes of Zeeman splitting

in the magnetic fields used in this work are larger than the assumed exciton fine structure splittings, so that states forming bright triplets would be effectively mixed, and the observed linewidths of reflectivity spectra are quite large also. Thus, we could not resolve the exciton fine structure in our experiments and we do not expect to have different reflectivity spectra for various crystal orientations. As it was shown in Ref. [S5], the exciton g -factor in CsPbBr₃ is almost isotropic and our neglecting of exciton fine structure while fitting experimental data is justified.

S2. Modeling of exciton-polaritons in reflectivity

Exciton-polaritons are quasiparticles created by light-matter interaction that couples excitons with photons. In semiconductors with sufficiently strong light-matter interaction such as CsPbBr₃, exciton-polaritons determine the optical properties in the vicinity of the exciton resonance. Their properties can be studied by measuring reflectivity spectra in this spectral range. The dispersion relation is:

$$\frac{c^2 k^2}{\omega^2} = \varepsilon(\omega, k), \quad (\text{S1})$$

where ω is the incident light frequency and \mathbf{k} is the light wave vector. The exciton-polaritons are characterized by the dependence of the dielectric function $\varepsilon(\omega, k)$ not only on the light frequency, but also on the wave vector, i.e. they exhibit spatial dispersion. Schematically the exciton-polariton dispersion is shown in Fig. 1(c) in the main text. Incident light with frequency ω gives rise to one or two polaritons (depending on ω) in the semiconductor crystal. Consequently, the boundary conditions for electromagnetic waves are insufficient to solve Maxwell's equations. One can, therefore, either solve the non-local Maxwell equations^{S6,S7} or introduce additional boundary conditions^{S8,S10}. For our study it is sufficient to use simple boundary conditions in the form of a “dead” layer^{S8}, a layer with thickness L near a semiconductor surface in which excitons can not exist.

Here we consider a normal incidence of light wave on a semi-infinite dielectric crystal. Near the exciton-polariton resonance if the electric field and exciton polarization are parallel or perpendicular to the light wave vector (for uniaxial crystals electric field has to be perpendicular or parallel to optical axis), the dielectric function in Eq. (S1) takes the form^{S8}:

$$\varepsilon(\omega, k) = \varepsilon_b + \frac{4\pi\alpha_0 E_T^2}{E_T^2 - \hbar^2\omega^2 + \frac{\hbar^2 k^2}{M} E_T - i\hbar^2\omega\Gamma}, \quad (\text{S2})$$

where E_T is the energy of the transverse (“mechanical”) exciton state in the absence of the spatial dispersion and with the resting center of masses, and \mathbf{k} is the exciton center of masses wave vector. Due to momentum conservation, exciton center of masses wave vector \mathbf{k} is equal to the wave vector of incident light. $M = m_e + m_h$ is the translation exciton mass with $m_{e(h)}$ being the electron (hole) effective mass. Note, that the electron and hole relative motion in the exciton is described by the reduced exciton mass μ , defined as $\mu^{-1} = m_e^{-1} + m_h^{-1}$. The parameter ε_b is the background dielectric constant at the energy of the exciton-polariton resonance, here we take it as a high frequency dielectric constant of the crystal. The parameter $4\pi\alpha_0$ is the exciton polarizability, which controls the exciton oscillator strength, and Γ is the damping. Parameter ε_b is the background dielectric constant on the frequency of excitonic transition without taking into account the exciton resonance. Note, that in literature on exciton-polaritons the background dielectric constant ε_b is sometimes labeled as ε_0 , see e.g. Refs. [S8] and [S9]. But this ε_0 should not be mixed with the stationary dielectric constant at zero frequency, as rather $\varepsilon_b \equiv \varepsilon_0 \approx \varepsilon_\infty$.

The exciton polarizability describes the efficiency of light-matter interactions resulting in mixing of the transverse and longitudinal modes of the exciton-polariton. It is connected with the longitudinal-transverse splitting energy $\hbar\omega_{LT}$ as^{S11,S10}:

$$\hbar\omega_{LT} = \frac{4\pi\alpha_0 E_T}{2\varepsilon_b}. \quad (\text{S3})$$

Then,

$$\varepsilon(\omega, k) = \varepsilon_b \left(1 + \frac{2\hbar\omega_{LT} E_T}{E_T^2 - \hbar^2\omega^2 + \frac{\hbar^2 k^2}{M} E_T - i\hbar^2\omega\Gamma} \right). \quad (\text{S4})$$

Solving the dispersion relation of exciton-polaritons, Eq. (S1), where $\varepsilon(\omega, k)$ is defined in Eq. (S2), we find the refractive index of the media. The resulting reflection coefficient is^{S11}:

$$R = \frac{1 - n^*}{1 + n^*}, \quad (\text{S5})$$

where the boundary conditions are taken into account in the form of the “dead” layer

$$n^* = \sqrt{\varepsilon_b} \left[\frac{(n^\dagger + \sqrt{\varepsilon_b})e^{-2ik\sqrt{\varepsilon_b}L} - \sqrt{\varepsilon_b} + n^\dagger}{(n^\dagger + \sqrt{\varepsilon_b})e^{-2ik\sqrt{\varepsilon_b}L} + \sqrt{\varepsilon_b} - n^\dagger} \right], \quad n^\dagger = \frac{n_1 n_2 + \varepsilon_b}{n_1 + n_2}, \quad (\text{S6})$$

where L is the thickness of the dead layer, and n_1 and n_2 are refractive indices found as roots of the dispersion relation (S1) and corresponding to the two lower and upper exciton-polariton branches. Substituting Eq. (S6) into Eq. (S5) we model the reflectivity spectra in the vicinity of the exciton-polariton resonance, which we treat as isolated and do not take into account possible overlap between different exciton states in the spectrum.

In our simplified model, the damping Γ describes the combined contribution of both homogeneous and inhomogeneous broadening. We assume that homogeneous broadening dominates in our case due to the high quality of the CsPbBr₃ crystal under study. We also neglect the complex conduction band structure, which is justified by the very large value of spin-orbit splitting $\Delta_{SO} = 1.5$ eV, and treat both the topmost valence band and the bottom conduction as isotropic and parabolic.

To fit the reflectivity spectrum in the vicinity of the exciton-polariton resonance we take M , E_T , $\hbar\omega_{LT}$, Γ , and L as the fitting parameters. The longitudinal exciton energy is calculated as $E_L = E_T + \hbar\omega_{LT}$. In calculations we take the background dielectric constant $\varepsilon_b = \varepsilon_\infty = 4.3$ from Ref. [S12].

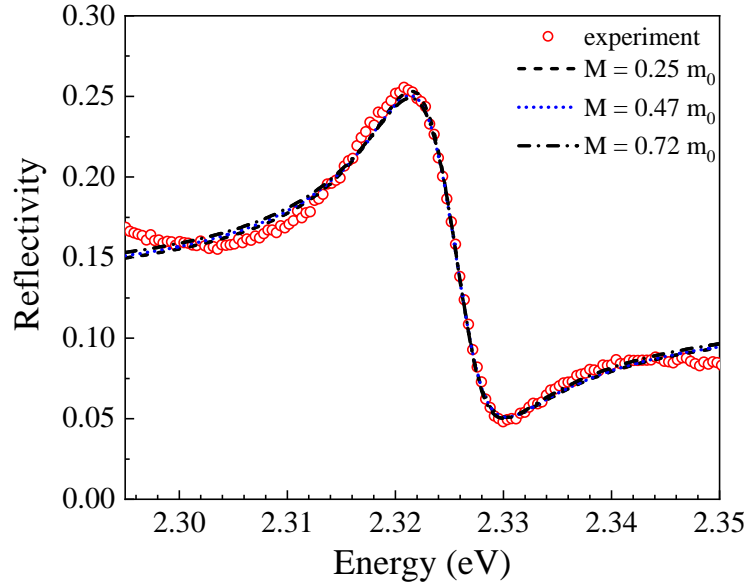


FIG. S2. Modeling of the exciton-polariton resonance measured in reflectivity (open circles) for a CsPbBr₃ crystal. Lines show calculation results using exciton translation masses of $M = 0.25m_0$, $0.47m_0$, and $0.72m_0$.

TABLE S1. Exciton-polariton parameters for CsPbBr₃ at $T = 1.6$ K as determined by modeling of the reflectivity spectrum in Figure S2.

M	E_T (eV)	$\hbar\omega_{LT}$ (meV)	Γ (meV)	L (nm)
$0.25m_0$	2.3219	5.4	6.2	3.1
$0.47m_0$	2.322	5.4	6.8	3.5
$0.72m_0$	2.322	5.3	6.7	2.3

The results of the fitting of reflectivity spectra in zero magnetic field with different translation exciton masses, M , are shown by lines in Fig. S2. For each fit we fixed M and varied other parameters. The best fit parameters are given in Table S1. One can see that the exciton parameters are only weakly sensitive to the choice of M , which was varied from $0.25m_0$ up to $0.72m_0$. The value of $M = 0.47m_0$ is in line with Refs. S1, S13, and S14. Solving equations (6), (7), (8), and (9) from the main text we unambiguously found the exciton reduced mass $\mu = 0.18m_0$. Then, considering that in the lead halide perovskites the electron and hole effective masses are close to each other,

we get $M \approx 4\mu = 0.72m_0$. Therefore, for all fits in various magnetic fields we use $M = 0.72m_0$. At zero magnetic field it gives us the following exciton-polariton parameters: $E_T = 2.322$ eV, $\hbar\omega_{LT} = 5.3$ meV, $\hbar\Gamma = 6.7$ meV, and $L = 2.3$ nm. The obtained dead layer thickness, although it is only a model parameter, is of similar magnitude as the exciton Bohr radius, which seems reasonable.

Note that the energy of transverse exciton, E_T , which is crucial for determination of the exciton parameters, shows almost no dependence on the exciton translation mass, and on other parameters showed only very slight dependence. Also, although we have several fitting parameters, most of them can be determined with a high accuracy, as they are individually responsible for specific aspects of the reflectivity spectrum: its spectral energy position, amplitude, shape, and line broadening (damping). Therefore, the obtained values of exciton parameters are reliable and are evaluated with high accuracy.

In Table S2 we summarize parameters measured and evaluated for CsPbBr₃ in this paper and give comments on how they were obtained.

TABLE S2. Exciton parameters in bulk CsPbBr₃ crystal. $T = 1.6$ K.

Parameter	Value	Comments
$E_T = E^{1S}$	2.3220 eV	Energy of transverse exciton. Obtained from the fit of reflectivity spectra.
E_L	2.3273 eV	Energy of longitudinal exciton. Calculated by expression $E_L = E_T + \hbar\omega_{LT}$.
$\hbar\omega_{LT}$	5.3 meV	Longitudinal-transverse splitting. Obtained from the fit of reflectivity spectra at zero magnetic field.
$\hbar\Gamma$	6.7 meV	Exciton damping. Obtained from the fit of reflectivity spectra at zero magnetic field.
$4\pi\alpha_0$	0.0195	Exciton polarizability. Calculated from Eq. (S3).
ε_b	4.3	Background dielectric constant. Taken as $\varepsilon_b = \varepsilon_\infty = 4.3$ from Ref. S12.
E^{2P}	2.3467	Energy of 2P exciton. Measured by two-photon absorption.
g_X	+2.35	Exciton g -factor. Obtained from experimentally measured Zeeman splitting of exciton, namely of E_T splitting in σ^+ and σ^- polarizations.
c_d^{1S}	1.6 $\mu\text{eV}/\text{T}^2$	Diamagnetic coefficient of 1S exciton. Obtained from fitting the center-of-gravity of dependence $E_T(B)$ in σ^+ and σ^- polarizations.
c_d^{2P}	10 $\mu\text{eV}/\text{T}^2$	Diamagnetic coefficient of 2P exciton. Obtained by fitting the energy shift of 2P exciton state in magnetic field measured by two-photon absorption.
E_b^{1S}	32.5 meV	Binding energy of 1S exciton state, i.e. the exciton Rydberg R^* in the hydrogen-like model. Calculated as $E_b^{1S} = E_g - E^{1S}$.
E_b^{2P}	7.8 meV	Binding energy of 2P exciton state. Calculated as $E_b^{2P} = E_g - E^{2P}$.
E_g	2.3545 eV	Band gap energy. Evaluated from experimental data.
ε_{eff}	8.7	Effective dielectric constant. Evaluated from experimental data.
μ	0.18 m_0	Reduced exciton mass. Evaluated from experimental data.
M	0.72 m_0	Translation exciton mass. Evaluated as $M = 4\mu$ suggesting that $m_e = m_h$.
a_B^{1S}	2.55 nm	Exciton Bohr radius. Evaluated from Eq. (3) using experimental data.

S3. Longitudinal-transverse splitting of excitons in lead halide perovskites

The valence band of lead halide perovskites is S-like (as are the conduction bands of III-V and II-IV semiconductors). The bottom conduction subband is an analog of spin-split valence subband of conventional semiconductors. In the quasicubical approximation the basis functions of the valence and conduction bands in perovskites are^{S3,S15}:

$$u_{v,+ \frac{1}{2}} = iS \uparrow, \quad u_{v,- \frac{1}{2}} = iS \downarrow, \quad (\text{S7})$$

$$u_{c,+ \frac{1}{2}} = -\frac{1}{\sqrt{3}}Z \uparrow - \frac{1}{\sqrt{3}}(X - iY) \downarrow, \quad u_{c,- \frac{1}{2}} = \frac{1}{\sqrt{3}}Z \downarrow - \frac{1}{\sqrt{3}}(X + iY) \uparrow \quad (\text{S8})$$

while basis functions of heavy electrons (analog of heavy holes) are^{S3,S15}:

$$u_{he,+ \frac{3}{2}} = -\frac{1}{\sqrt{2}}(X + iY) \uparrow, \quad u_{he,- \frac{3}{2}} = -\frac{1}{\sqrt{2}}(X - iY) \downarrow, \quad (\text{S9})$$

where X , Y and Z are functions of p-orbitals forming the conduction bands of perovskites.

The interband momentum matrix element P_{cv} is defined as

$$P_{cv} = \langle S | \hat{p}_x | X \rangle = \langle S | \hat{p}_y | Y \rangle = \langle S | \hat{p}_z | Z \rangle, \quad (\text{S10})$$

where $\hat{p}_{x,y,z}$ are components of the momentum operator. We are considering σ^\pm polarized light, so we are interested in excitons with dipole moments along x and y . To calculate the matrix element of interaction with light one has to consider functions (S9) or (S10). The Kane energy E_p is connected with P_{cv} as

$$E_p = \frac{2P_{cv}^2}{m_0}. \quad (\text{S11})$$

From one point the exciton longitudinal-transverse splitting is the consequence of the long-range part of the exchange interaction^{S16,S17}, from the other it is connected to the exciton oscillator strength, describing the exciton contribution to the polarization induced by incoming light. Calculating the excitonic contribution to polarization analogously to Ref. [S18] we arrive to

$$\hbar\omega_{LT} = \frac{4e^2\hbar^2}{3m_0E_T^2} \frac{E_p}{\epsilon_b a_B^3}, \quad (\text{S12})$$

Note, that there is additional factor “2/3” as compared with Ref. [S18] due to the perovskite band structure.

In the quasicubical approximation the effective masses of electrons and hole can be calculated as^{S3}:

$$\frac{1}{m_e} = \frac{1}{m_0} + \frac{E_p}{3m_0E_g}, \quad \frac{1}{m_h} = \frac{1}{m_0} - \frac{E_p(3E_g + \Delta)}{3m_0E_g(E_g + \Delta)}, \quad (\text{S13})$$

where Δ is the spin orbit splitting of the conduction band in the quasicubical approximation. One can estimate the Kane energy E_p both from Eq. (S12) and from Eq. (S13). Respective numbers are given in main text.

-
- * dmitri.yakovlev@tu-dortmund.de
- ^{S1} C. C. Stoumpos, C. D. Malliakas, J. A. Peters, Z. Liu, M. Sebastian, J. Im, T. C. Chasapis, A. C. Wibowo, D. Y. Chung, A. J. Freeman, B. W. Wessels and M. G. Kanatzidis, Crystal growth of the perovskite semiconductor CsPbBr₃: A new material for high-energy radiation detection. *Crystal Growth & Design* **2013**, *13*, 2722.
- ^{S2} J. Even, L. Pedesseau, M.-A. Dupertuis, J.-M. Jancu, and C. Katan, Electronic model for self-assembled hybrid organic/perovskite semiconductors: Reverse band edge electronic states ordering and spin-orbit coupling. *Phys. Rev. B* **2012**, *86*, 205301.
- ^{S3} E. Kirstein, D. R. Yakovlev, M. M. Glazov, E. A. Zhukov, D. Kudlacik, I. V. Kalitukha, V. F. Sapega, G. S. Dimitriev, M. A. Semina, M. O. Nestoklon, E. L. Ivchenko, N. E. Kopteva, D. N. Dirin, O. Nazarenko, M. V. Kovalenko, A. Baumann, J. Höcker, V. Dyakonov, M. Bayer, The Landé factors of electrons and holes in lead halide perovskites: universal dependence on the band gap. *Nat. Commun.* **2022**, *13*, 3062.
- ^{S4} M. Baranowski, K. Galkowski, A. Surrente, J. Urban, L. Klopotoski, S. Maćkowski, D. Kennedy Maude, R. Ben Aich, K. Boujdaria, M. Chamarro, C. Testelin, P. K. Nayak, M. Dollmann, H. J. Snaith, R. John Nicholas, and P. Plochocka, Giant fine structure splitting of the bright exciton in a bulk MAPbBr₃ single crystal. *Nano Lett.* **2019**, *19*, 7054.
- ^{S5} N. E. Kopteva, D. R. Yakovlev, E. Kirstein, E. A. Zhukov, D. Kudlacik, I. V. Kalitukha, V. F. Sapega, O. Hordiichuk, D. N. Dirin, M. V. Kovalenko, A. Baumann, J. Höcker, V. Dyakonov, S. A. Crooker, M. Bayer, Weak dispersion of exciton Landé factor with band gap energy in lead halide perovskites: Approximate compensation of the electron and hole dependences. arXiv:2301.12775 (2023).
- ^{S6} A. A. Maradudin and D. L. Mills, Effect of the spatial dispersion on the properties of a semi-infinite dielectric. *Phys. Rev. B* **1973**, *7*, 2787.
- ^{S7} G. S. Agarwal, D. N. Pattanayak, and E. Wolf, Electromagnetic fields in spatially dispersive media. *Phys. Rev. B* **1974**, *10*, 1447.
- ^{S8} J. J. Hopfield and D. G. Thomas, Theoretical and experimental effects of spatial dispersion on the optical properties of crystals. *Phys. Rev.* **1963**, *132*, 563.
- ^{S9} A. A. Maradudin and D. L. Mills, Effect of Spatial Dispersion on the Properties of a Semi-Infinite Dielectric. *Phys. Rev. B* **1973**, *7*, 2787.
- ^{S10} D. D. Sell, S. E. Stokowski, R. Dingle, and J. V. DiLorenzo, Polariton reflectance and photoluminescence in high-purity GaAs. *Phys. Rev. B* **1973**, *7*, 4568.
- ^{S11} J. J. Hopfield and D. G. Thomas, On some observable properties of longitudinal excitons. *J. Phys. Chem. Solids* **1960**, *12*, 276–284.
- ^{S12} K. Miyata, D. Meggiolaro, M. T. Trinh, P. P. Joshi, E. Mosconi, S. C. Jones, F. De Angelis, and X.-Y. Zhu, Large polarons in lead halide perovskites. *Sci. Adv.* **2017**, *3*, e1701217.

- ^{S13} Z. Yang, A. Surrente, K. Galkowski, A. Miyata, O. Portugall, R. J. Sutton, A. A. Haghighirad, H. J. Snaith, D. K. Maude, P. Plochocka, and R. J. Nicholas, Impact of the halide cage on the electronic properties of fully inorganic cesium lead halide perovskites. *ACS Energy Lett.* **2017**, *2*, 1621.
- ^{S14} G. R. Yettapu, D. Talukdar, S. Sarkar, A. Swarnkar, A. Nag, P. Ghosh, and P. Mandal, Terahertz conductivity within colloidal CsPbBr₃ perovskite nanocrystals: remarkably high carrier mobilities and large diffusion lengths. *Nano Lett.* **2016**, *16*, 4838.
- ^{S15} Z. G. Yu, Effective-mass model and magneto-optical properties in hybrid perovskites. *Scientific Reports* **2016**, *6*, 28576.
- ^{S16} M. M. Denisov and V. P. Makarov, Longitudinal and transverse excitons in semiconductors. *Phys. Stat. Sol. (b)* **1973**, *56*, 9.
- ^{S17} L. C. Andreani, F. Bassani, and A. Quattropani, Longitudinal-transverse splitting in Wannier excitons and polariton states. *il Nuovo Cimento D* **1988**, *10*, 1473.
- ^{S18} E. L. Ivchenko, *Optical Spectroscopy of Semiconductor Nanostructures* (Springer, Berlin 2007).
-